Photon transfer in a system of coupled superconducting microwave resonators

Colclough, Mark; Muirhead, Christopher; Gunupudi, Bindu-Malini

DOI:
10.1063/1.4961593

AIP Journal of Applied Physics

Photon transfer in a system of coupled superconducting microwave resonators

C. M. Muirhead, B. Gunupudi, and M. S. Colclough

Citation: Journal of Applied Physics **120**, 084904 (2016); doi: 10.1063/1.4961593
View online: http://dx.doi.org/10.1063/1.4961593
View Table of Contents: http://scitation.aip.org/content/aip/journal/jap/120/8?ver=pdfcov
Published by the AIP Publishing

Photon transfer in a system of coupled superconducting microwave resonators

C. M. Muirhead,[a] B. Gunupudi, and M. S. Colclough
School of Physics and Astronomy, University of Birmingham, Edgbaston, Birmingham B15 2TT, United Kingdom

(Received 13 June 2016; accepted 12 August 2016; published online 24 August 2016)

A novel scheme is proposed for the study of energy transfer in a pair of coupled thin film superconducting microwave resonators. We show that the transfer could be achieved by modulating the kinetic inductance and that this has a number of advantages over earlier theoretical and experimental schemes, which use modulation of capacitance by vibrating nanobars or membranes. We show that the proposed scheme lends itself to the study of the classical analogues of Rabi and Landau-Zener-Stueckelberg oscillations and Landau-Zener transitions using experimentally achievable parameters. We consider a number of ways in which energy transfer (photon shuttle) between the two resonators could be achieved experimentally. *Published by AIP Publishing.*
[http://dx.doi.org/10.1063/1.4961593]

I. INTRODUCTION

The coupling of electromagnetic to mechanical motion at or approaching the quantum level has been the subject of much theoretical and experimental work in the last two decades. This has been driven partly by the wish to understand the basic physics of such interactions and partly by the goal of developing quantum information technology.[1,2] Much of the work has been carried out in optical resonators but, more recently, thin film superconducting resonators, working at microwave frequencies, have been extensively studied.[3–7] Microwave resonators have the advantage that they are more easily cooled into the quantum regime and are well fit for coupling to other quantum elements such as qubits,[8] quantum dots,[9] and data transmission lines.[10] They can also be driven nonlinear[11] more easily than in optical experiments, leading to a range of more complex behaviours. A proposal has been made,[12] but not yet realised, that two identical weakly coupled coplanar microwave resonators (CPRs) could have their resonant frequencies modulated by capacitive coupling to a nano-mechanical element (NE). This would induce energy exchange between the resonators, thus facilitating a study of a range of behaviours normally studied by optical means.[13] It would, however, involve sub-micron lithography and also it is not clear in Reference 12 how the NE would be driven in order to achieve sufficient simultaneous coupling to both resonators. It would also limit the modulation frequency to the mechanical resonant frequency of the NE in order that a sufficiently large amplitude of modulation could be obtained. The main proposal of this paper is that, instead of modulating the resonant frequencies by capacitive coupling to an NE, the proposed experiment could be achieved by modulating the Kinetic Inductance (KI) using known techniques[14,15] and, furthermore, that this could be done using realistically achievable experimental parameters. This would provide a powerful additional tool for studies of the classical analogues of a number of interesting processes, which have been extensively studied in the quantum regime, such as Landau-Zener transitions[16,17] (LZ) and Landau-Zener-Stueckelberg (LZS) oscillations.[18] When a quantum system is swept through an avoided crossing once (LZ) or in an oscillatory fashion (LZS), the system can remain in the same state or transition almost perfectly into another one, depending on the speed/frequency at which this is done. Analogous effects occur in coupled harmonic modes of a classical system, although we should emphasise that coupled oscillators differ from two level quantum systems in a number of important respects, e.g., the classical oscillators do not exhibit spontaneous emission and there is no relaxation due to phase decoherence. In this paper, we will use the terms "LZ-like transition," etc., to emphasise this distinction. LZ analogues have been demonstrated in coupled optical systems[19,20] and in coupled vibrational modes of a single nanobar.[21] Recent theoretical work has investigated the possible use of mechanically driven membranes separating two optical cavities to control LZ- and LZS-like dynamics[22] and to achieve controlled photon transfer between the cavities (photon shuttle). Very recently, LZS-like oscillations have been demonstrated in the single nanobar system.[23] Although these, and our proposed experiments, are analogues of quantum processes, as noted, coplanar resonators can easily be cooled into the sub-photon per resonator limit, and the effects considered here could be transferred into the quantum regime. The KI may be modulated by application of a magnetic field[14] or by applying a current.[15] The physics is closely related, although the experimental techniques are different. Lossless field tuning of single niobium CPRs with $Q \sim 10^6$ has already been demonstrated,[14] albeit with rather small (~2 MHz) frequency modulation, and high Q's have also been shown in a pair of weakly coupled niobium CPRs.[24] Much larger (1–200 MHz) frequency changes with Q up to 2×10^5 have been demonstrated in lumped element[25] and microstrip geometries for *single* NbTi resonators using current driven modulation.[15] This larger modulation is, in

[a]Electronic mail: c.m.muirhead@bham.ac.uk

part, due to the use of superconductors with a larger KI fraction and, in part, the different current distributions in the microstrip geometry.

In Section II, we outline the basics of the proposed experiment. In Section III, we show the results of our simulations for realistic experimental parameters. In Section IV, we consider the practicality of our proposed scheme in terms of the experimental design and the measurement system, and discuss some advantages and disadvantages of current driven modulation.

II. BASIC PRINCIPLE OF PROPOSED EXPERIMENTS

In Fig. 1, we show four suggested layouts for the proposed experiment. These all comprise two, notionally identical, weakly coupled microwave resonators. We discuss the designs in more detail below. For computational purposes, and to keep the analysis independent of any particular physical structure, we have modelled the coupled resonators as two bulk LCR circuits coupled by a weak capacitance C_k and driven from a constant current source. The output is open circuit. This therefore models an experiment in which the coupling to the external circuitry via the C_c's is sufficiently weak that the quality factor (Q) of the resonators approximates to the intrinsic value (Q_i). The behaviour of coupled resonators is well known in many branches of physics and engineering and results in an avoided crossing in the resonant frequencies when the two resonators have the same uncoupled resonant frequency. The behaviour is shown schematically in Figs. 2(b) and 2(c) for the cases where L_1 only is changed by ΔL_1 while L_2 remains constant (linear case) and where $\Delta L_2 = -\Delta L_1$ (quadratic case). The frequency splitting $f_{splitting} = f_U - f_L$ has a minimum value at the middle of the avoided crossing where the uncoupled frequencies of the two resonators are equal. For weak coupling (small C_k), this minimum value of $f_{splitting}$ is closely proportional to C_k.

The total inductance of a superconducting resonator $L = L_g + L_{KI}$, where L_g is the geometric inductance associated with the magnetic field energy and L_{KI} is the kinetic inductance associated with the kinetic energy of the Cooper pairs. L_{KI} increases as the square of the local magnetic field[14] and the local current density.[15,26] For $L_{KI}/L \ll 1$, this results in a resonant frequency $f(H)/f(0) = 1 - (H/H^*)^2$ or $f(I)/f(0) = 1 - (I/I^*)^2$, respectively, where H* and I* are materials, geometry, and temperature dependent parameters.

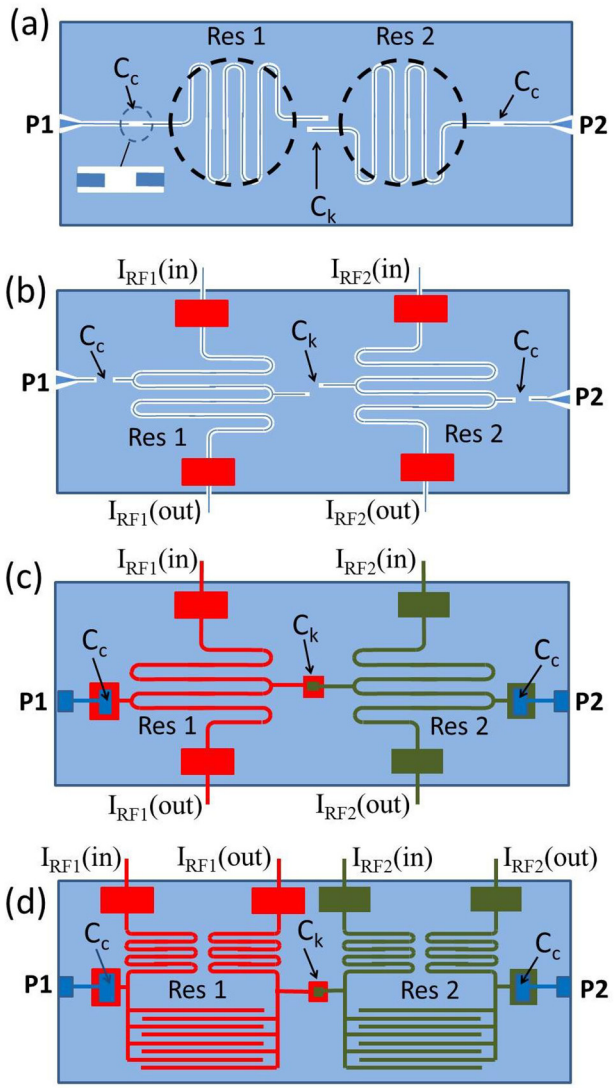

FIG. 1. Four schematic structures for a pair of weakly coupled thin film resonators. P1 and P2 are the microwave input and output ports. (a) Conventional CPRs designed for field modulation. (b) Conventional CPRs designed for current modulation; (c) as (a) only in microstrip configuration (i.e., with thin low loss dielectric film on top of superconducting ground plane; (d) as (c) only with lumped inductor/capacitors. In (b), (c), and (d), the large upper and lower rectangular sections are capacitive pads to ground. For details, see text and References 15 and 25. C_c and C_k are capacitive coupling pads.

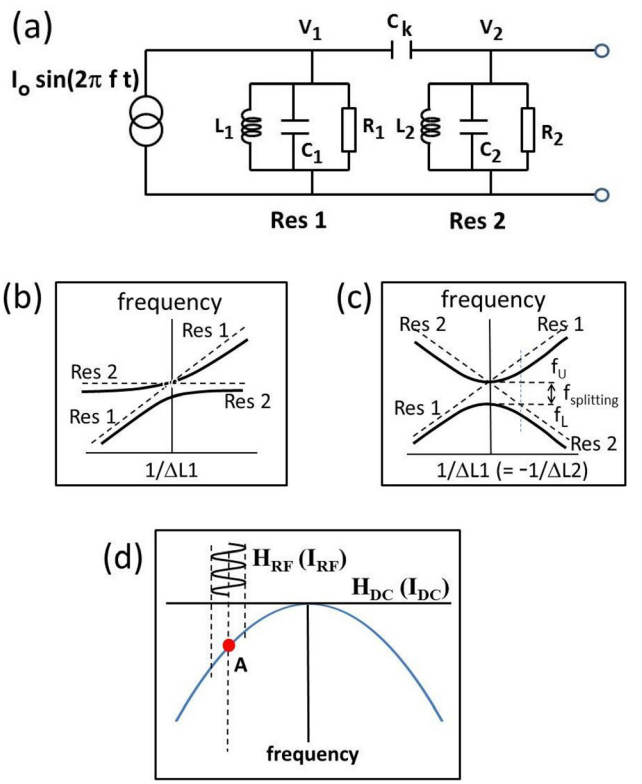

FIG. 2. Schematics of proposed experiment. (a) Equivalent circuit of the coupled resonators. (b) and (c) Frequency responses of the output signals when the individual kinetic inductances are changed. (b) For the case where only the inductance of Res 1 is changed and (c) when the inductance of both resonators are changed in antiphase. (d) Resonant frequency of a single resonator showing parabolic dependence on applied magnetic field or current.

The resonant frequency may therefore be controlled by application of an external magnetic field or by application of a current. In Fig. 2(d), we show the dependence of the resonant frequency of a coplanar resonator on a steady field H_{DC} applied perpendicular to the resonator plane, or on an applied current I_{DC}.

We now bias the system to point A and apply a small sinusoidal radio frequency (RF) modulation $H_{RF}(I_{RF})$ whose frequency is comparable with $f_{splitting}$. For generality, we refer to the steady and RF modulations as DC_{mod} and RF_{mod}, respectively. ΔL_1 and ΔL_2 have both linear and quadratic dependence on RF_{mod}, but we will find that we can easily arrange that the contribution to V_2 from the quadratic component is well outside our range of measurement. RF_{mod} may be applied to one resonator or antiphase to both resonators. The latter corresponds most closely to the optical case of two near identical cavities separated by an externally driven, weakly transparent membrane. The resonant frequency of one cavity is increased, and the other simultaneously decreased as the membrane moves. The quadratic case is, therefore, the one we will assume in our simulations. We find that the effect of applying RF_{mod} to Res 1 or Res 2 only is a reduction in the output signal of a factor close to 2. The detailed form of the response is also slightly modified.

We now consider the four proposed structures in Fig. 1 in more detail. The simplest, but least practical for integration into more complex structures, is the conventional CPR geometry in (a) which is designed for modulation by magnetic fields H_{DC} and H_{RF}. H_{DC} can be applied external to the cryostat and H_{RF} via small (~few mm) coils underneath the sample (shown as dotted circles). An integrated thin film coil could be used at a cost of more complex lithography and a reduction in Q as the coupling of the resonators to the environment was enhanced. Both H_{DC} and H_{RF} are applied perpendicular to the plane in order to take advantage of the large flux focussing factor (~w/t), where w is the track width and t is the film thickness. H is largest in the same region of the film as the microwave currents, i.e., along the resonator track edges,[27] and so the effect of H on the resonant frequency is maximal.

When $\mu_0 H$ at the film edges reaches the critical field $\mu_0 H_{C1}$ (~0.1 mT for niobium), flux lines enter the film, the field dependence becomes hysteretic, and the resonator Q drops. As a consequence of the large flux focussing factor this translates, for niobium films thick compared with the penetration depth, to a maximum applied field ~200 μT and a corresponding maximum frequency shift of 2 MHz,[14] much less than that potentially achievable in the stripline geometries below. The advantages of field modulation are (i) it is particularly simple, needing only patterning of a single layer; (ii) for fields less than the critical value, there is virtually no damping due to the external circuitry. Loaded Q as high as 10^6 has been demonstrated for a single CPR with no observable reduction for field less than H_{C1}, so we could expect to achieve similar behaviour in the coupled geometry.

A number of groups have recently demonstrated the shift of resonant frequency in single resonators in a microstrip[15] and lumped microstrip[25] configuration by increasing the KI with an applied current rather than an applied field. This has been achieved by connecting the resonator ends to ground with a large capacitance and driving the resonators near the middle, also by capacitive coupling. The effect is that the half wave resonators have voltage nodes at the ends, as opposed to the conventional CPR in (a), which has voltage antinodes. With high quality thin dielectric layers and careful capacitor design, Q's approaching 2×10^5 and frequency shift ~200 MHz have been achieved.[25] This sort of structure offers a more flexible approach than the simplistic flux modulation above, although we note that hysteresis and its associated losses does not seem to have been investigated in current driven structures, which must also be subject to flux ingression, degradation of the Q, and associated flux noise if the local field is allowed to exceed H_{C1}. The suppression of the order parameter, which causes the increase in KI, will also enhance the density of quasiparticles if operating at higher temperatures. Such effects are absent in nanomechanical elements.

Figs. 1(b)–1(d) show possible adaptations of this technique to coupled pairs of coplanar, microstrip, and lumped microstrip resonators geometries, respectively. Note that extended structures (not shown in (b)–(d)) are required to achieve low loss current connections (see Refs. 15 and 25 for more detail).

III. COMPUTER SIMULATIONS

In this section, we show the computed resonator responses primarily in the time domain and model a number of experiments that could be performed. We choose a set of parameters, which we will show are realistic and we have used these same parameters for the various experiments we are proposing. The splitting, RF frequency, DC, and RF amplitude are all under experimental control and could be adjusted to examine particular features in more detail. We have assumed a set of "worst case" parameters in that we have used up to the maximum demonstrated frequency shift for field tuning (2 MHz) and the maximum demonstrated Q for current tuning (2×10^5). For simplicity of presentation and computational time, we do not allow the resonator voltages to completely reach the steady state before showing the effect of applying an RF modulation of the inductances. For most experiments of interest, we would allow the steady state conditions to be reached first. The time derivative of the microwave drive current is

$$I' = 2\pi f I_0 \sin 2\pi f t, \tag{1}$$

and the equations of motion for the two resonators are

$$I' = V_1/L_1(1 + d\sin 2\pi f_{RF} t) + V_1'/R_1 + C_1 V_1'' + C_k(V_1'' - V_2''), \tag{2}$$

$$V_2/L_2(1 - d\sin 2\pi f_{RF} t) + V_2'/R_2 + C_2 V_2'' = C_k(V_1'' - V_2''). \tag{3}$$

We take $L_1 = L_2$, $C_1 = C_2$, and $R_1 = R_2$ unless otherwise stated so that we are at the middle of the avoided crossing. Putting $d = 0$ (no rf drive), we turn I_0 on at time $t = 0$ at a frequency $f = f_L$ and turn I_0 off at time $t_a = 30\,\mu s$. We solve Eqs. (1)–(3) numerically to obtain the response of V_1 and V_2 in the time domain (Figs. 3(a) and 3(b), respectively).

The responses of V_1 and V_2 are identical in magnitude as expected, although the response at the microwave frequencies is in-phase when driven at f_L and out of-phase when driven at f_U. We see the expected rising and falling relaxation times due to the finite Q. If we allow t_a to become long compared with the relaxation time, we can integrate over the last part of the data to obtain the response in the steady state. We show the steady state value of V_{2rms} as a function of frequency in Fig. 3(d). We see that the peaks in (d) are around 8% higher than the maxima reached in (a) and (b), reflecting the fact that V_1 and V_2 do not quite reach the steady state. Very similar factors are obtained in the other non-steady state responses shown in Figs. 4–6. We find excellent agreement of the steady state response in Fig. 3(d) with results from the linear response circuit simulator SPICE.[28]

We concentrate on V_{2rms} since this is proportional to the output voltage and, as we will see in Section IV, our proposed measurement scheme provides an output proportional to the rms voltage of the microwave oscillations. $(V_{2rms})^2$ is also analogous to the transfer coefficient in coupled mode optical experiments.

A. Bloch oscillations and splitting of the resonance peaks

We first drive the system at frequency f_U, turning off the microwave drive at 30 μs. For $t > 30\,\mu s$, we now modulate the inductances at frequency f_{RF} chosen to be equal to

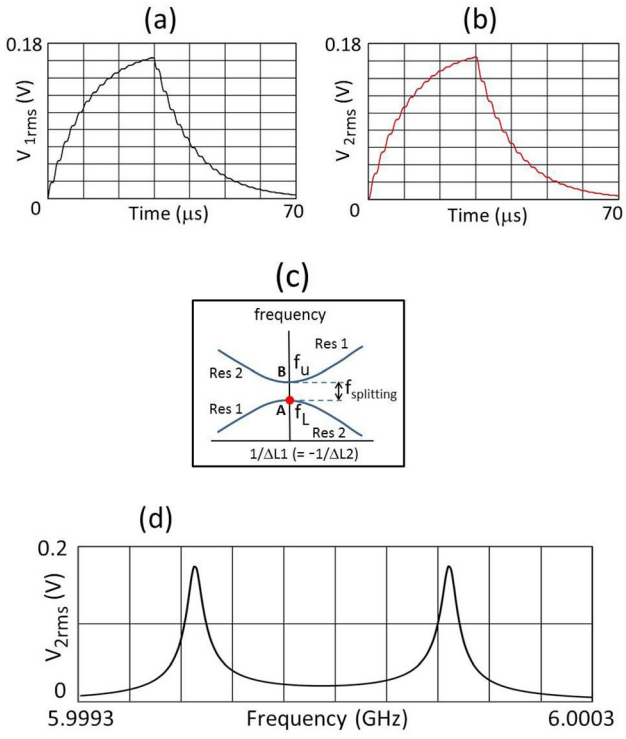

FIG. 3. (a) V_{1rms} versus time and (b) V_{2rms} versus time, for two identical resonators when the system is driven at the lower resonant frequency, f_L (point A in (c)) from $t = 0$ to $t = 30\,\mu s$. (d) V_{2rms} versus frequency in the steady state. We have set $L_1 = L_2 = 1.29139 \times 10^{-9}$ H; $C_1 = C_2 = 5.4485 \times 10^{-13}$ F, which are in the same proportion as a typical 6 GHz CPR; $C_k = 4.5 \times 10^{-17}$ F; $R_1 = R_2 = 10^7\,\Omega$. These values correspond to $Q = 2 \times 10^5$ and a splitting frequency $f_{splitting} = 0.498$ MHz at the middle of the avoided crossing. I_0 has been taken as $5 \times 10^{-8}\,A_{rms}$ (see Section IV).

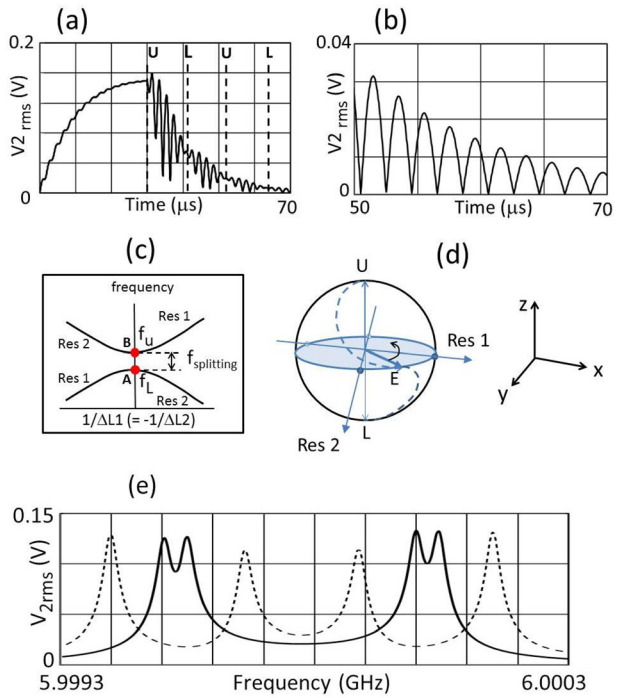

FIG. 4. (a) and (b) Time response of V_{2rms} when the system is driven at a microwave frequency f_U (Point B in 4(c)) from 0 to 30 μs. For $t > 30\,\mu s$, the inductances of the two resonators are modulated in anti-phase at the splitting frequency $f_{splitting} = 0.498$ MHz with an amplitude $d = 1.5 \times 10^{-5}$ (equivalent to 45 kHz). All other parameters are as in Fig. 3. (c) Expanded time responses after setting $d = 0$ for $t > 47\,\mu s$. (d) Bloch sphere representation of the behaviour. The surface is defined by a vector of length E. In a non-rotating frame, E spirals around the z-axis at a frequency $f_{splitting}$ as it moves sinusoidally between U and V at f_{Rabi}. When E lies on the equator, the energy oscillates between Res 1 (x-direction) and Res 2 (y-direction). (e) Frequency response of V_{2rms} in the steady state showing Autler-Townes-like splitting. The solid line is for a drive amplitude $d = 1.5 \times 10^{-5}$ and the dotted line for an amplitude $d = 9 \times 10^{-5}$.

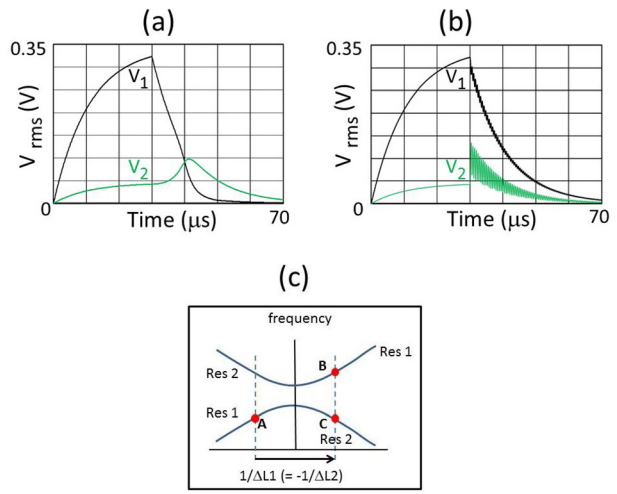

FIG. 5. (a) and (b) Swept (LZ-like) transitions showing the voltage in the two resonators. The system is excited at point A in (c). After 30 μs the microwave drive is turned off and the field is swept so as to take the inductances linearly in time between the left and right vertical dotted lines ($d = 3.1 \times 10^{-4}$). (a) For a sweep time = 10×, the inverse splitting frequency at the middle of the avoided crossing and (b) a sweep time = 0.1× the inverse spitting frequency.

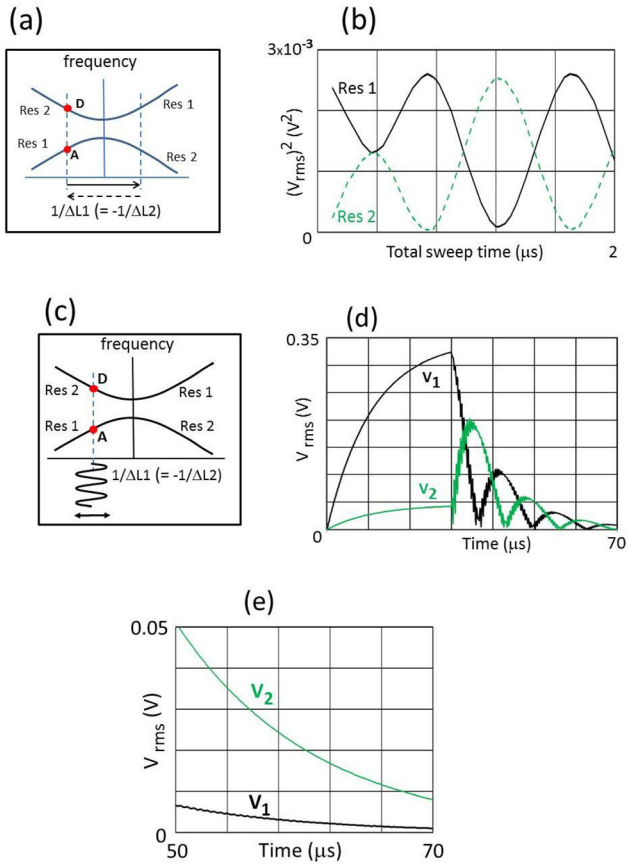

FIG. 6. Periodically driven transitions. (a) We first follow the process for an LZ-like transition shown in Fig. 5. The ramp direction is then reversed to bring the system back to the left hand vertical dotted line. (b) V^2 as a function of total ramp time. (c) The system is excited at the frequency of point A, where $f_B - f_A$ is 1.9 MHz, 4× greater than $f_{splitting}$. After 30 μs, the microwave drive is turned off and RF_{mod} at $d = 10^{-4}$ is applied at the new splitting frequency. (d) Time evolution of the occupancies of Res 1 and Res 2. (e) Effect of subsequently turning off the RF drive at 48.8 μs where the voltage across Res 1 is a minimum.

$f_{splitting} = f_U - f_L$; $L_1 = L_{10}(1 + d \sin 2\pi f_{RF} t)$; and $L_2 = L_{20}(1 - d \sin 2\pi f_{RF} t)$, i.e., in antiphase. d is directly proportional to the linear component in $f(RF_{mod})$ and here has a value giving a frequency modulation small compared with $f_{splitting}$. We observe envelopes at two new frequencies superimposed on the exponential decay (Fig. 4(a)).

The behaviour is most easily understood in the Bloch sphere representation shown in Fig. 4(d), where we have used a non-rotating reference frame. We start by exciting the system at the upper frequency f_U, so that the vector E points in the +z direction at point U. V_1 and V_2 are antiphase at the microwave frequency f_U and the current through the coupling capacitor C_k is maximal. The microwave drive is now turned off and, initially, we will assume no damping (infinite Q). L_1 and L_2 are now driven antiphase at the RF frequency f_{RF}. E spirals along the dotted path to the lower resonant frequency f_L at point L, where V_1 and V_2 are in-phase at the microwave frequency and the current in C_k is zero. If the RF drive is maintained, E moves cyclically between L & U at the Classical Rabi frequency ($f_{Rabi} \propto d \sim 45$ kHz) while simultaneously cycling around the z-axis at the beat frequency, $f_{splitting}/2$ (~0.25 MHz). In Fig. 4(a), the dotted vertical lines show the corresponding points U and L on the Bloch sphere.

The detailed form of the dotted line in Fig. 4(d) clearly depends on the relationship of these two frequencies. In the presence of damping, the Bloch sphere (and hence all observable voltages) shrinks exponentially with time. Fig. 4(b) shows the effect of turning off the RF drive after a $3\pi/2$ rotation into the equatorial plane and the energy oscillates cyclically between the two resonators at a frequency $f_{splitting}$. If we leave I_0 on while simultaneously applying RF_{mod} we can again obtain the frequency response in the steady state and find splitting of the f_L and f_U peaks by a frequency f_{Rabi}. The splitting is comparable with a linewidth reflecting the behaviour in the time domain and is closely proportional to the RF modulation amplitude. This is the classical analogue of Autler-Townes[29] splitting in a 2-level quantum system. We see that by increasing d, larger splitting can easily be obtained (dashed line). For $d > 1.5 \times 10^{-4}$, the peaks overlap and the behaviour becomes more complex.

In order to transfer energy from one resonator to the other and retain that state (subject to the overall exponential decay), we must bias the resonators away from the avoided crossing as shown by the vertical dotted lines in Fig. 5(c). As we move further from the middle of the avoided crossing, the occupancies of the upper and lower frequencies have less antisymmetric and symmetric character and become progressively identified with the occupancy of Res 1 and Res 2. This can be achieved by changing L_1 and L_2 by equal and opposite amounts. There are two related techniques that we can use in order to obtain a transfer between the two resonators: swept transitions and periodically driven transitions.

B. Swept transitions between resonators

Landau-Zener transitions are of great importance in quantum systems[16,17] when the sweep of an external parameter takes a system through an avoided crossing. If the sweep rate is low, the system remains on the initial branch and, if fast, there is a transition between the two branches. The time scale is set by the splitting frequency. We now look at the possibility of observing LZ-like transitions between the two resonators. We start by applying DC_{mod} to take the system to point A in Fig. 5(c). We see (Figs. 5(a) and 5(b)) that initially Res 1 (nearest to the microwave drive) is driven to an amplitude ≈8 times that of Res 2. At $t = 30$ μs, we turn off I_0 and sweep the inductances at a steady rate between values shown by the left and right dotted lines. In Fig. 5(a), we show the result of sweeping through the avoided crossing in a time long compared with the minimum inverse splitting frequency ($\tau_{sweep} = 10\tau_{splitting}$). The system remains in the lower branch (adiabatic transition) and the energy transfers from Res 1 to Res 2. The ratio $V_2/V_1 \approx 8$ giving an energy transfer ratio ($\propto V^2$) is ≈64: this corresponds in the quantum limit to a 98% probability of an energy transfer (photon shuttle) between the two resonators. In Fig. 5(b), we show the result of sweeping through the transition in a time short compared with the inverse splitting frequency ($0.1\tau_{splitting}$). The system crosses to the upper branch and the energy remains dominantly in Res 1 (diabatic transfer) as expected. We also see additional fast oscillations in both resonators. These are found to be antiphase and of equal magnitude when V^2

(proportional to the energy) is plotted, rather than V (not shown). They result from Fourier components at $f_{splitting}$ present in the fast sweep of the inductances. We note that, with the slow sweep we require for energy transfer between the two resonators, the responses are pleasingly smooth. Although we have described the offset process in terms of an increase in L_1 and a decrease in L_2, any combination of L_1 and L_2 can be thought of as an equal and opposite displacement of L_1 and L_2 from the middle of an avoided crossing. This could be achieved with a combination of DC_{mod} and RF_{mod}. The responses shown in Figs. 5(a) and 5(b) have used a DC_{mod} equivalent to (±900 kHz), around half the maximum that can be obtained with a magnetic field. Significantly larger energy transfers between the two resonators could clearly be achieved using current tuning.

C. Periodically driven transitions between resonators

The LZ-like transition yields a monotonic transition between the slow (A → C) and fast (A → B) paths. A more complex situation arises when the external parameter is swept repetitively between the two vertical dotted lines in Fig. 6(c) at a frequency comparable with the splitting frequency. In each successive crossing, the upper and lower energy states undergo a phase shift, which is cumulative and this results in an oscillatory dependence of the occupancies of the two resonators. In Fig. 6, we start with the procedure shown in Fig. 5(c), exciting the system at point A and sweeping linearly to the right dotted line and immediately reversing the sweep at the same rate to bring the system back to the left-hand dotted line. In Fig. 6(b), we plot the occupancy of the two resonators (Res 1 at point A and Res 2 at Point D) as a function of the total sweep time. In a quantum system, these are the Landau-Zener-Stueckelberg oscillations. Here, we have plotted V^2 to show that the energy is conserved. We see that, by choosing the total sweep time, we can move photons back and forward between the two resonators in a controlled fashion. Again there are oscillations at $f_{splitting}$ which have been averaged to obtain the smooth curves in Fig. 6(b). LZS-like oscillations have been very recently demonstrated experimentally in the coupled vibrational modes of a nanobar.[21]

Alternatively, we can use a sinusoidal oscillation to achieve a similar effect. In Fig. 6(d), we show the effect of applying RF_{mod} after exciting at point A for 30 ms. Again, we find that the occupancy of the two resonators oscillates periodically as a function of time and may be interrupted to put the energy dominantly in one or other resonator. We note that it is not necessary to actually traverse the avoided crossing to obtain the effect shown in Fig. 6(e): it is only necessary for the system to spend a significant fraction of the sweep time in the vicinity of the crossing for cumulative phase shifts to occur. We also note that the most complete transfer between the resonators, as shown in Fig. 6(d) is obtained when f_{RF} is chosen to be equal to $f_D - f_A$. This may be thought of as Rabi-like splitting at high drive level. In contrast to Rabi-like splitting at the middle of the avoided crossing (Fig. 4(b)), the energy transferred remains in the new state after the sweep has terminated.

IV. ANALYSIS OF EXPERIMENTAL FEATURES

The first requirement is for the resonant frequencies of Res 1 and Res 2 to be matched within a precision of $f_{splitting}$ which we have taken to be ∼0.5 MHz. This is $\sim 10^{-4}$ of the microwave frequency, and it is very hard to achieve this degree of accuracy without recourse to some *in-situ* tuning system. Reference 30 has shown differences of up to 30 MHz for two weakly coupled CPRs fabricated on the same chip. This is far too large to be achievable with magnetic tuning, but is well within the range of current tuning as long as hysteresis at this level does not become an issue. A number of other techniques have been described in the literature, involving piezoelectric and ferroelectric layers,[31] magnetic field controlled SQUIDs,[32] voltage controlled paddles,[33] current controlled KI,[15] and simple mechanical tuning.[24] The first three compromise the Q and, in the case of SQUIDs or paddles, requires multiple patterning so, mechanical tuning would be the simplest method, although this would not lend itself to integration with more complex structures.

Our proposal for the detection system is that the microwave output be rectified by a simple mixer whose signal and local oscillator inputs are both driven by the detected output V_0. The square root of this signal would compare directly with the rms output plotted in our simulations. The quadratic component of the field response would give a signal at twice the microwave frequency and would be easily filtered out. There are a number of other parameters which must be considered. Kinetic inductance effects at the microwave frequency place a limit on the microwave current and hence the output voltage V_2 which, for a simple CPR design, we deduce from the data to be ∼0.25 V_{rms}.[30] We have set the microwave input current to 2.5×10^{-8} A in our simulations to keep below this value. The coupling capacitors C_c are limited to $\sim 5 \times 10^{-16}$ F to avoid significantly reducing the loaded Q below Q_i. If, in addition, we assume a 10 dB loss in the microwave cable to the top of the cryostat, this translates to a maximum output voltage $V_0 \sim 450\,\mu V_{rms}$. We could expect to be looking for signals down to a few percent of this to cover the experiments of interest, say, $10\,\mu V_{rms}$, which would be amplified either internal or external to the cryostat. There are two unwanted signals. First, the thermal noise which, for a 50 Ω line at room temperature is ∼1nV/rtHz. Our shortest timescale is 2 μs, so a measurement bandwidth of about 50 MHz would be required to resolve this. This gives a thermal noise magnitude of $7\,\mu V_{rms}$, comparable with our smallest signal level. 10^4 averages (time ∼1–10 s) would, therefore, give a percent accuracy. There are a range of low temperature amplifiers available, with noise temperatures down to 5 K in microwave frequency range of interest, which would reduce the number of averages by a factor ∼10. Second, there is inevitably some breakthrough signal in the experimental chamber which underlies the resonant peak and which cannot be removed by low temperature amplification or by averaging. References 34 and 35 report this as 50 dB below the resonant peak value, which translates to just 0.3% of the maximum signal level.

We note a particular issue with coplanar designs, whether magnetic field or current driven. The wire bonds connecting

the ground plane to the underlying printed circuit board serve to reduce the RF currents flowing around the outer surface of the ground plane (and hence the flux applied to the resonator) at frequencies above R/L where R is a typical wire bond resistance and L is the inductance of a resonator. R/L can easily be <1 MHz. At frequency above R/L, the effective RF_{mod} is reduced approximately in inverse proportion to the frequency. These problems can be addressed by making the transmission line between the wire bonds and the C_c gaps sufficiently long that it has an inductance equal to that of a resonator (not shown in Fig. 1). This limits the reduction in circulating current at RF frequencies to a factor of 2 below the maximum, which we can easily accommodate.

The current driven stripline designs of Figs. 2(c) and 2(d) offer much higher magnitudes for DC_{mod} and RF_{mod}, allowing larger $f_{splitting}$, and/or much bigger frequency shifts which, in turn, would enable larger photon transfer ratios between the two resonators. As noted above, the maximum frequency shifts are limited by the point at which the applied current or magnetic field induces magnetic flux in the superconductor. This, in turn, limits the maximum current density. Microstrip designs typically have a capacitance to ground 1–2 orders of magnitude larger than the coplanar designs for a given resonant frequency and, hence, a correspondingly smaller output voltage for a given total current and Q. The current is, however, distributed over the track width, w, rather than its thickness, t, so, for penetration depth small compared with the film thickness, we would expect a current enhancement $\sim w/2t \sim 50$ for a given maximum current density. The overall trade off will depend on the film thickness and the materials used for both the superconductor and the dielectric layers.

V. SUMMARY AND CONCLUSIONS

We have used simulations to demonstrate how the modulation of inductance by means of a combination of steady and radio-frequency magnetic fields or currents could be used to transfer energy between a pair of superconducting microwave resonators in a controlled way using experimentally achievable parameters. This is a more versatile technique than the use of nanobars or membranes and would provide a powerful tool for the study of the classical analogues of Rabi and LZS oscillations and LZ transitions. We have assumed worst case values for DC_{mod} and RF_{mod}, so there are good prospects of being able to extend the proposed experiments to a much wider range of parameters, although we note that such extensions require the demonstration that hysteresis and the concomitant problems of Q degradation and flux noise are not an issue. Despite their other disadvantages, nanobars and membranes do not have these limitations. Our proposed method also has a number of advantages over the use of optical cavities in that microwave resonators can easily be cooled into the sub-photon per resonator state and would lend themselves well to integration with other thin film quantum structures, where transfer and storage of microwave photons plays a particularly important role. By increasing the microwave drive, the system could be driven non-linear, leading to a range of more complex behaviours. It would also be easy to extend the techniques to multiple coupled resonators or, by coupling to other harmonics, to facilitate studies of multimode systems.

ACKNOWLEDGMENTS

We wish to acknowledge the support from EPSRC and the University of Birmingham for a College Elite Scholarship for B. Gunupudi. We are grateful to Andrew Armour for his helpful comments on an earlier draft.

[1]F. Nori and J. You, in *Principles and Methods of Quantum Information Technologies* (Springer, 2016), pp. 461–476.
[2]M. Aspelmeyer, T. J. Kippenberg, and F. Marquardt, Rev. Mod. Phys. **86**, 1391 (2014).
[3]J. D. Teufel, F. Lecocq, and R. W. Simmonds, Phys. Rev. Lett. **116**, 013602 (2016).
[4]T. Kipf and G. S. Agarwal, Phys. Rev. A **90**, 053808 (2014).
[5]M. Yuan, V. Singh, Y. M. Blanter, and G. A. Steele, Nat. Commun. **6**, 8491 (2015).
[6]C. A. Holmes, C. P. Meaney, and G. J. Milburn, Phys. Rev. E **85**, 066203 (2012).
[7]T. Palomaki, J. Harlow, J. Teufel, R. Simmonds, and K. Lehnert, Nature **495**, 210 (2013).
[8]S. Zeytinoğlu, M. Pechal, S. Berger, A. Abdumalikov, Jr., A. Wallraff, and S. Filipp, Phys. Rev. A **91**, 043846 (2015).
[9]T. Frey, P. J. Leek, M. Beck, A. Blais, T. Ihn, K. Ensslin, and A. Wallraff, Phys. Rev. Lett. **108**, 046807 (2012).
[10]G. Cataldo, E. J. Wollack, E. M. Barrentine, A. D. Brown, S. H. Moseley, and K. U-Yen, Rev. Sci. Instrum. **86**, 013103 (2015).
[11]E. A. Tholén, A. Ergül, K. Stannigel, C. Hutter, and D. B. Haviland, Phys. Scr. **2009**, 014019.
[12]G. Heinrich and F. Marquardt, Europhys. Lett. **93**, 18003 (2011).
[13]M. Metcalfe, Appl. Phys. Rev. **1**, 031105 (2014).
[14]J. Healey, T. Lindström, M. Colclough, C. Muirhead, and A. Y. Tzalenchuk, Appl. Phys. Lett. **93**, 043513 (2008).
[15]A. Adamyan, S. Kubatkin, and A. Danilov, Appl. Phys. Lett. **108**, 172601 (2016).
[16]L. D. Landau, "Zur theorie der energieubertragung, II." Phys. Sov. Union **2**, 46 (1932).
[17]C. Zener, Proc. R. Soc. London, Ser. A **137**, 696–702 (1932).
[18]S. Shevchenko, S. Ashhab, and F. Nori, Phys. Rep. **492**, 1 (2010).
[19]R. Spreeuw, N. Van Druten, M. Beijersbergen, E. Eliel, and J. Woerdman, Phys. Rev. Lett. **65**, 2642 (1990).
[20]D. Bouwmeester, N. Dekker, F. v. Dorsselaer, C. Schrama, P. Visser, and J. Woerdman, Phys. Rev. A **51**, 646 (1995).
[21]M. J. Seitner, H. Ribeiro, J. Kölbl, T. Faust, J. P. Kotthaus, and E. M. Weig, preprint arXiv:1602.01034 (2016).
[22]G. Heinrich, J. Harris, and F. Marquardt, Phys. Rev. A **81**, 011801 (2010).
[23]T. Faust, J. Rieger, M. J. Seitner, J. P. Kotthaus, and E. M. Weig, Nat. Phys. **9**, 485 (2013).
[24]B. Gunupudi, C. Muirhead, and M. Colclough, Rev. Sci. Instrum. **87**, 014707 (2016).
[25]M. R. Vissers, J. Hubmayr, M. Sandberg, S. Chaudhuri, C. Bockstiegel, and J. Gao, Appl. Phys. Lett. **107**, 062601 (2015).
[26]J. Zmuidzinas, Annu. Rev. Condens. Matter Phys. **3**, 169 (2012).
[27]A. Porch, P. Mauskopf, S. Doyle, and C. Dunscombe, IEEE Trans. Appl. Supercond. **15**, 552 (2005).
[28]T. A. Fjeldly, M. Shur, and T. Ytterdal, *Introduction to Device Modeling and Circuit Simulation* (John Wiley & Sons, Inc., 1997).
[29]S. H. Autler and C. H. Townes, Phys. Rev. **100**, 703 (1955).
[30]B. Gunupudi, "Coupled superconducting microwave resonators for studies of electro-mechanical interaction," Ph.D. thesis (University of Birmingham, 2015).
[31]J. Sok, J. Lee, and E. Lee, Supercond. Sci. Technol. **11**, 875 (1998).
[32]Z. Wang, Y. Zhong, L. He, H. Wang, J. M. Martinis, A. Cleland, and Q. Xie, Appl. Phys. Lett. **102**, 163503 (2013).
[33]Z. Kim, C. Vlahacos, J. Hoffman, J. Grover, K. Voigt, B. Cooper, C. Ballard, B. Palmer, M. Hafezi, J. Taylor *et al.*, AIP Adv. **1**, 042107 (2011).
[34]J. Hornibrook, E. Mitchell, and D. Reilly, IEEE Trans. Appl. Supercond. **23**, 1501604 (2013).
[35]J. Hornibrook, E. Mitchell, C. Lewis, and D. Reilly, Phys. Procedia **36**, 187 (2012).